Juan Du
Graduate School of Chinese Academy of Sciences,
Beijing 100190, China;
Institute of Engineering Thermophysics,
Chinese Academy of Sciences,
Beijing 100190, China;
Key Laboratory of Advanced Energy and Power,
IET, CAS,
Beijing 100190, China

Feng Lin
Tri-State University,
Angola, IN 46703

Hongwu Zhang

Jingyi Chen

Institute of Engineering Thermophysics,
Chinese Academy of Sciences,
Beijing 100080, China;
Key Laboratory of Advanced Energy and Power,
CAS,
Beijing 100080, China

Numerical Investigation on the Self-Induced Unsteadiness in Tip Leakage Flow for a Transonic Fan Rotor

A numerical investigation on the self-induced unsteadiness in tip leakage flow is presented for a transonic fan rotor. NASA Rotor 67 is chosen as the computational model. It is found that under certain conditions the self-induced unsteadiness can be originated from the interaction of two important driving "forces:" the incoming main flow and the tip leakage flow. Among all the simulated cases, the self-induced unsteadiness exists when the size of the tip clearance is equal to or larger than the design tip clearance. The originating mechanism of the unsteadiness is clarified through time-dependent internal flow patterns in the rotor tip region. It is demonstrated that when strong enough, the tip leakage flow impinges the pressure side of neighboring blade and alters the blade loading significantly. The blade loading in turn changes the strength of the tip leakage flow and results in a flow oscillation with a typical signature frequency. This periodic process is further illustrated by the time-space relation between the driving forces. A correlation based on the momentum ratio of tip leakage flow over the incoming main flow at the tip region is used as an indicator for the onset of the self-induced unsteadiness in tip leakage flow. It is discussed that the interaction between shock wave and tip leakage vortex does not initiate the self-induced unsteadiness, but might be the cause of other types of unsteadiness, such as broad-banded turbulence unsteadiness. [DOI: 10.1115/1.3145103]

1 Introduction

Unsteady flows in the tip region are one of the sources of noise, blade vibration, and flow losses in compressors [1]. In some cases, unsteady tip leakage flow was demonstrated to potentially link to stall inception [2,3]. Although the tip leakage flow has been under extensive studies for many years, its unsteadiness is a recent focus in axial compressor research community [2–11]. Three types of unsteadiness have been reported, which are given as follows.

- *Induced vortex*. In 1999, Mailach [4] reported a phenomenon with oscillatory tip leakage vortex rotating from blade to blade while the compressor still operated in a near stall but stable operating point. This phenomenon is referred to as "rotating instability." A series of papers were then published by Mailach thereafter in regards to rotating instability. In 2001, Marz et al. [5] performed a detailed unsteady casing pressure measurement and a time-accurate numerical simulation for the full annulus of a low-speed axial compressor. The mechanism of rotating instability was attributed to an induced vortex when it travels from suction side to pressure side at roughly half of the rotor speed. Bergner et al. [6] and Hah et al. [7] experimentally and numerically investigated a high-speed transonic compressor stage, respectively. The oscillation in tip leakage flow was also found. This oscillation was attributed to an induced vortex and the shock-vortex interaction.
- *Vortex breakdown*. Furakawa et al. recognized the role of tip leakage vortex breakdown in compressor aerodynamics [8] and further indicated that the breakdown could be one of the sources of unsteadiness in tip leakage flow [9]. The work was extended to a transonic compressor by Yamada et al. [10].
- *Self-induced unsteadiness*. Zhang et al. [11] found a new type of unsteadiness. The tip leakage flow could become unsteady at high loading operating conditions without involving multiblades in a low-speed compressor rotor. Because this type of the unsteadiness is a result of interaction of incoming main flow and tip leakage flow, we call it self-induced unsteadiness. Tong et al. [3] experimentally demonstrated its existence. They also found that spike was initiated at the circumferential location with the strongest unsteadiness.

This paper will extend the study of self-induced unsteadiness to a high-speed compressor. The research questions are the following.

(1) Does the self-induced unsteadiness exist in high-speed rotors? If yes, what are the phenomena?
(2) What is the originating mechanism of the self-induced unsteadiness in high-speed rotors?

This paper is organized as follows. After a brief introduction of NASA Rotor 67 and the computational fluid dynamics (CFD) scheme, the results of CFD are validated with the available experimental results. Having evidenced the location and frequency of the unsteadiness of tip leakage flow, we carefully examine the instantaneous flow fields and clarify the mechanism of the self-induced unsteady tip leakage flow for this rotor. The proposed mechanism is also supported by studying the influence of tip clearance sizes while keeping the incoming main flow unchanged. The results show that the self-induced unsteadiness in tip leakage flow in this high-speed rotor is due to the dynamic interaction of the same two driving "forces" as those in low-speed compressor [11,12]. A correlation based on the momentum ratio of these two driving forces, the tip leakage flow over the incoming main flow at the tip region, is worked out and used as an indicator for the

Contributed by the International Gas Turbine Institute of ASME for publication in the JOURNAL OF TURBOMACHINERY. Manuscript received August 14, 2008; final manuscript received February 23, 2009; published online January 20, 2010. Review conducted by David Wisler. Paper presented at the ASME Turbo Expo 2008: Land, Sea and Air (GT2008), Berlin, Germany, June 9–13, 2008.

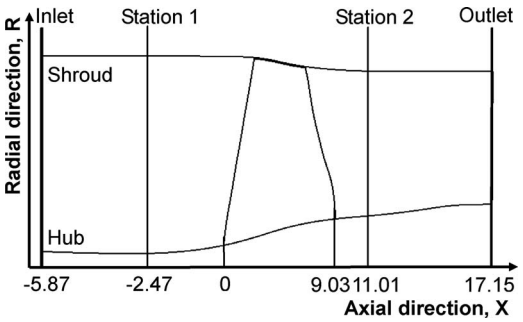

Fig. 1 Measurement location and computation region

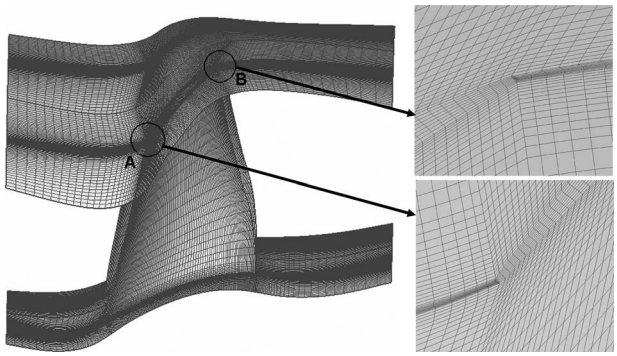

Fig. 2 Computational geometry and grid distribution for Rotor 67

onset of the self-induced unsteadiness. Before concluding the paper, the role of shock wave in regards to the unsteadiness of tip leakage flow and the link of this flow unsteadiness to stall inception are discussed.

2 Rotor 67 and the Numerical Scheme

2.1 Basic Parameters of the Transonic Fan Rotor. NASA Rotor 67, the first stage rotor of a two-stage fan, is a low-aspect-ratio design, which is designed for axial inflow without an inlet guide vane. It had been selected as a computed target to investigate the strong interaction between the tip leakage vortex and the in-passage shock wave by Adamczyk [13]. In this paper, Rotor 67 is used for unsteady investigation of tip leakage flow. The specifications and measurement data of Rotor 67 can be found in Ref. [14].

2.2 Numerical Tool and Computation Scheme. Unsteady flow simulations were performed by solving unsteady three-dimensional, Reynolds-averaged Navier–Stokes equations. A commercial solver package, FLUENT, was utilized for the present work. The solver is a three-dimensional, time-accurate code with implicit second-order scheme. The standard κ-ε turbulence model and standard wall function were used to account for the turbulence flow. Standard and realizable κ-ε turbulence model were compared with improving precision of computation. The comparison between numerical and experimental results demonstrated that the prediction by applying standard κ-ε turbulence model is better. Several numerical researches using this unsteady flow solver have been conducted for low-speed and high-speed compressor rotors [11,12,15], and the computation results matched with experiments well.

It has been shown that in low-speed compressors, the self-induced unsteady tip leakage flow can be simulated using single blade passage computation model [12]. In other words, this kind of unsteadiness can be triggered without invoking cross-blade passage flows, such as leading spillage of tip leakage vortex, reversed flow, and so on. In order to verify this observation in high-speed rotors, self-induced unsteadiness in multipassage environment (five blade passages or 5/22 of the Rotor 67 annulus) is also investigated. The results at the design tip clearance are shown in the Appendix, which clearly demonstrates that the characteristics for all the blade passages are identical while the self-induced unsteadiness is captured. Hence, the computation model in this paper is chosen as a single blade passage model. The computation domain with inlet and outlet axial coordinates is shown in Fig. 1. Total pressure, total temperature, and flow angles were given uniformly at the inlet boundary. Static pressure was specified with simple radial equilibrium law at outlet. Nonslip and adiabatic conditions were imposed on all solid walls.

Figure 2 presents the rotor geometry and grid distribution. The grid resolution for a single blade passage is a structured H-mesh with 160 nodes (80 nodes on the blade) streamwise, 54 nodes pitchwise, and 70 nodes in the spanwise direction. 8, 10, and 16 nodes are applied in the tip clearances of 0.25%, 1.1%, and 2.2% blade tip chords, respectively.

2.3 Validation of Simulation. In order to validate numerical simulation in the present work, the results of simulation are compared with experimental results. The comparison of adiabatic efficiency is depicted in Fig. 3, while that of the total pressure ratio characteristic is presented in Fig. 5. Points I and II are the operating conditions near peak efficiency and near stall, respectively. The numerical results follow the same trend as the experiments, although the discrepancy slightly increases at small normalized mass flow rates. Our discrepancy is of the same order as the discrepancy in other studies. Figure 4 showed the blade-to-blade plots of relative Mach number contours at 90% span from hub for two operating conditions. The Mach number contours, in which the location of the shock waves is clearly displayed, match reasonably well with each other.

Grid independence had also been tested. Although we obtained 0.9% improvement in total pressure ratio prediction, there was no qualitative difference by doubling current numbers of grid cells. Since we will focus on the qualitative unsteady features in the rest of this paper, we decide to use current numbers of grid cells $(160\times54\times70)$ for unsteady simulation for the benefit of shorter simulation time.

3 Results

3.1 The Locations and Frequency of Unsteady TLF. Numerical simulations were carried out for three different tip clearance sizes. Figure 5 depicts the characteristics for each tip clearance. The simulations for this isolated rotor were run at the design rotational speed with various back pressures. All mass flow rates were normalized by the value at choke. Several points are labeled

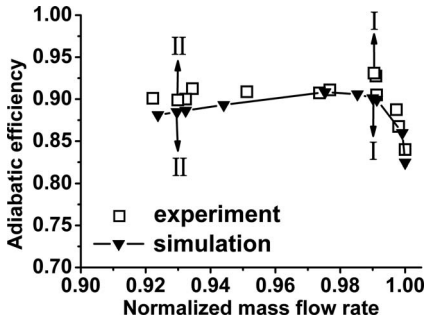

Fig. 3 Computed and measured adiabatic efficiency characteristic for design tip clearance. (*a*) Operating condition near peak efficiency (Point I). (*b*) Operating condition near stall (Point II).

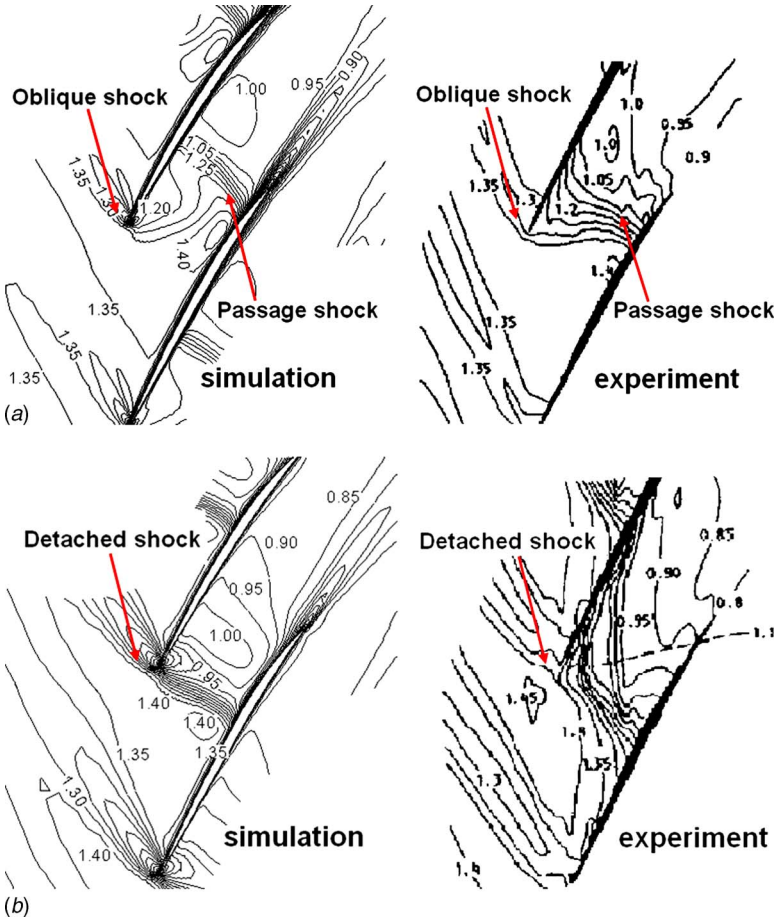

Fig. 4 Comparison of computed and measured relative Mach number at 90% span from hub for design tip clearance

in Fig. 5 for later convenience, among which letters S, U, N, and T are used to represent steady, unsteady, next-to-near-stall, and near-stall operating points, respectively. Subscripts 1, 2, and 3 are for 0.25%, 1.1%, and 2.2% tip chord of tip clearances, respectively. Note that near-stall points are those with highest back pressure before the iterative process diverges. For the design value of 1.1% tip chord, the only unsteady tip leakage flow case happens at the near-stall point. For 0.25% tip chord, unsteady computational results demonstrate that there is no unsteadiness of tip leakage flow. For 2.2% tip chord, unsteadiness is found long before the near-stall point. The first such point is then labeled as U_3 in Fig. 5.

Figure 6 depicts the static pressure root-mean-square (rms) distribution for Rotor 67 at operating point T_2. LE, TE, PS, and SS are abbreviations for leading edge, trailing edge, pressure surface, and suction surface, respectively. The high static pressure rms regions are concentrated on the tip region, and the rms of static pressure at the pressure side is of an order higher than that at the suction side. This result demonstrates that the unsteadiness under investigation is a tip-sensitive phenomenon.

A total of 24 monitoring points are located along the blade surface at 99% span, half of which are set on the pressure side, and half on the suction side. The fast Fourier transform results for the pressure at the points on the pressure side are given in Fig. 7. The magnitude of oscillation on the suction side of blade

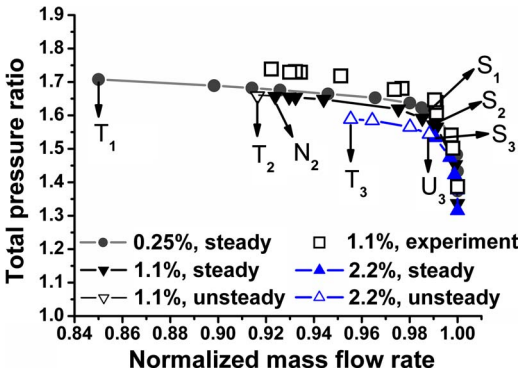

Fig. 5 Computed total pressure ratio characteristic for three tip clearance sizes

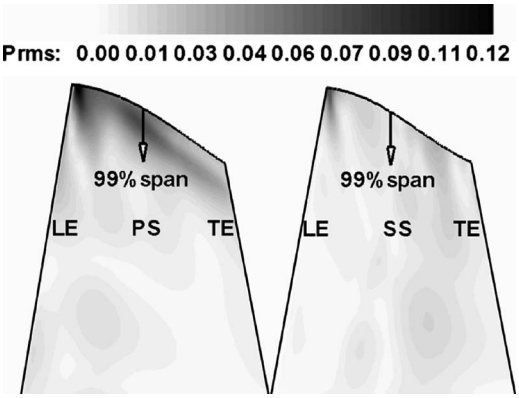

Fig. 6 Static pressure rms distribution for Rotor 67 at T_2

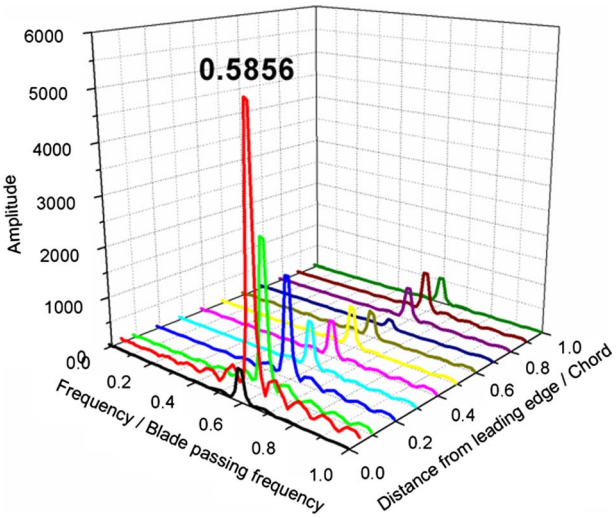

Fig. 7 Frequency and amplitude characteristics in the rotor tip region at 99% span

is too weak to display. The oscillation frequency is 0.5856 blade passing frequency (BPF) for all points, which is fairly close to the results of a low-speed rotor in Ref. [12] and a transonic rotor (Rotor 37) in Ref. [15]. The pressure at 7% tip chord from leading edge fluctuates stronger than any other point.

3.2 The Instantaneous Flow Fields and the Flow Mechanism. The instantaneous flow fields in the rotor tip region are closely examined in order to clarify the originating mechanism of the self-induced unsteadiness. Three types of graphs and curves are used, each of which contains its own information. The contours of static pressure coefficient (C_p) are a classic way used by many researchers to depict the tip leakage vortex trajectory and the shock wave in the flow field. The contour plots of relative total pressure coefficient (C_{rtp}) reveal the influences of low-energy flows because the difference in C_{rtp} along the axial direction is related to the shaft work added onto the flow. The curves of static pressure coefficient distribution along the pressure side are given to clearly display the propagation of low-pressure spot.

Figure 8 lists all three types of graphs and curves side by side for six time instants within one period of fluctuation for the design tip clearance of 1.1% tip chord at near-stall operating condition (Point T_2 in Fig. 5). All of them are taken from the cross section at 99% span (right at the tip of the blade). Note that we have mentioned that the frequency of this unsteadiness is 0.5856 BPF, which corresponds to a period of 1.7 T. Therefore, the last instant, $t=(50/30)T=1.67$ T, is quite close to the first instant.

Before further describing the flow structure in Fig. 8, it is necessary to introduce the interface between the incoming main flow and the tip leakage flow. This interface can be easily identified from the relative total pressure plots (Fig. 8(*b*)). Before the inter-

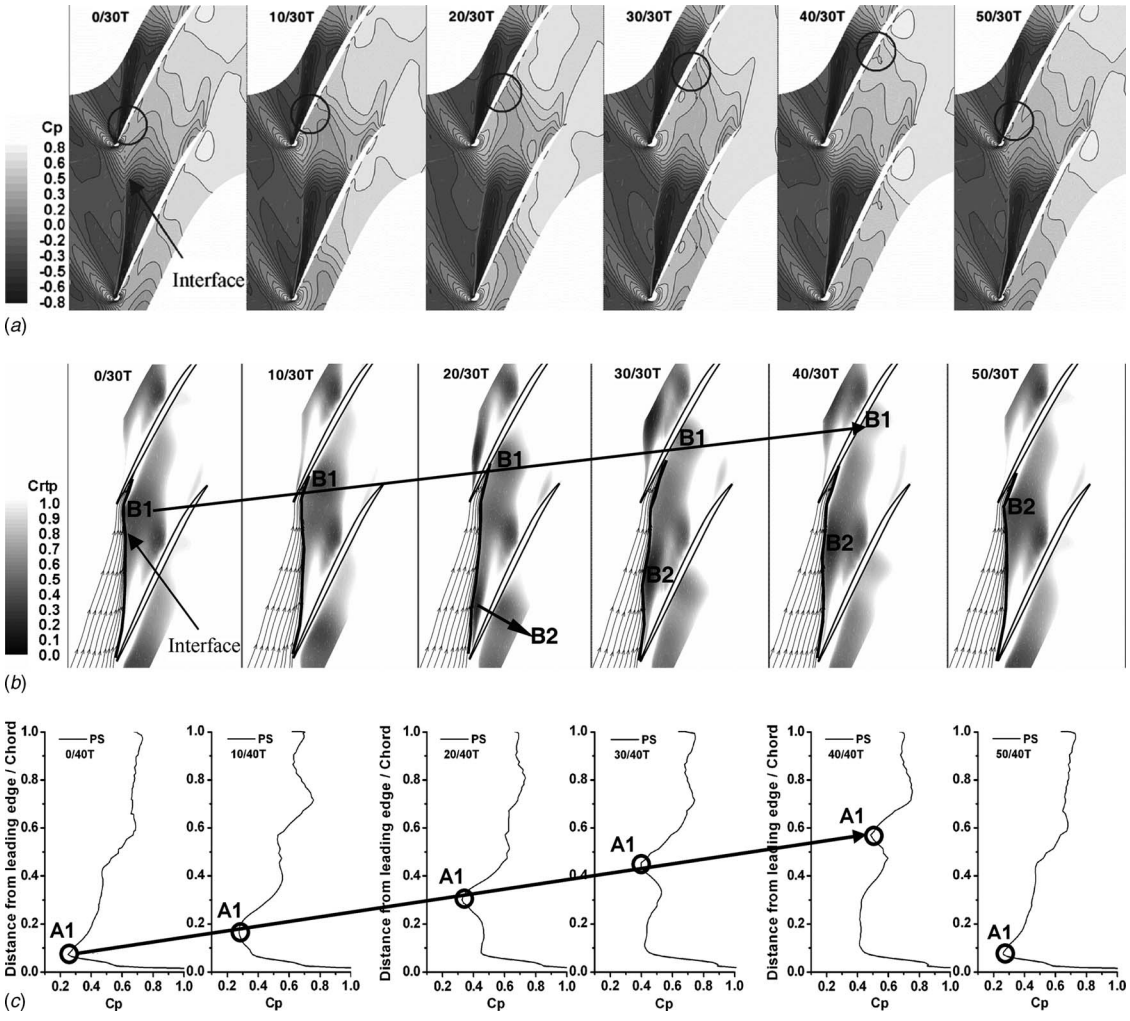

Fig. 8 Instant plots taken from 99% span at T_2 operating condition. (*a*) Static pressure coefficient. (*b*) Relative total pressure coefficient. (*c*) Pressure coefficient distribution on blade pressure surface.

face, it belongs to the incoming flow; after the interface, it is dominated by the tip leakage flow (there may exist some main flows leaking through the boundary layer of the suction side, but they are too weak compared with the tip leakage flow in this region). Since the tip leakage flow does not take any shaft work as energy input (that is why they are called "leakage flow"), their relative total pressure values are low. Therefore, the region influenced by the tip leakage flow can be easily identified in the relative total pressure plot (bounded by the interface lines in Fig. 8(*b*)). Streamlines from incoming main flow are added onto the plots in Fig. 8(*b*), so that one can simultaneously see how incoming flow and the tip leakage flow behave.

The identified interface is then added on the static pressure contours in Fig. 8(*a*) with its one end truncated so that the pressure field near the pressure surface can be seen clearly without interference. The interface is not the trajectory of the vortex, but it follows the tip leakage vortex and extends toward the pressure side of the neighboring blade. If this interface cannot stretch all the way across the blade passage, the incoming main flow can still go through the blade passage and establish a complete circulation around the tip region of the blade. The pressure difference across both sides of the blade is not disturbed, which in turn maintains a steady tip leakage flow. The whole flow field is thus steady.

Once the interface is able to go across the blade passage and reach the pressure side, one of the two possible scenarios may occur. One is that the tip leakage flow is too weak to create a large region of influence. The other is just the opposite: The tip leakage flow behind the interface is strong enough to influence the pressure distribution on the pressure side significantly. For the first scenario, the tip leakage flow is still steady because the incoming main flow dominates. The examples of this scenario can be seen in Figs. 12(*a*), 12(*b*), and 13(*a*) later in this paper. For the second scenario, however, the dynamic interaction between the incoming main flow and the tip leakage flow changes significantly. Figure 8 depicts the second scenario.

Unless otherwise noted, the region of influence by the tip leakage flow can be identified as a low relative total pressure region in Fig. 8(*b*). Due to the facts that the interface goes across the blade passage and that the tip leakage flow behind it is strong, the incoming main flow is blocked by the interface and is directed toward the pressure side of the blade (as seen in Fig. 8(*b*)). The main flow then creates a stagnating high-pressure spot near the leading edge on the pressure side before the interface, followed by the low-pressure spot behind the interface. The low-pressure spot is actually a part of the region of influence by the tip leakage flow, labeled as circle A1 in Fig. 8(*c*). The high-pressure spot pushes the adjacent low-pressure spot downstream (marked by the arrow line) and initiates the unsteadiness. For convenience, the time-dependent process of the low-energy tip leakage flow along the blade pressure surface (B1) and across the blade passage (B2), and the corresponding pressure variation process on the pressure surface (A1), as shown in Fig. 8, is summarized schematically in Fig. 9.

There are two time axes in Fig. 9. The one along the blade chord represents the time instants at which the low-energy spot (B1) and low-pressure spot (A1) propagate along the blade pressure side. The process of the low-energy tip leakage flow (B2) traveling across the blade passage is timed accordingly at the vertical axis. It can be seen that within the same time period, there are two streams of low-energy spots (B1 and B2) and one stream of low-pressure spots (A1). Each low-energy spot on the pressure side (B1) matches with the low-pressure spot (A1) nicely at the same chord location at the same time instant, inferring both are under the influence from the tip leakage flow. Through observing Fig. 9, there are two mechanisms in forming the time-dependent process of the tip leakage flow that need further elaboration. (1) As mentioned above, due to the effect of incoming main flow, the high-pressure spot stretches and pushes the low-pressure spot downstream along the pressure surface. So how will this alter the blade loading and thus create a reaction on the tip leakage flow? (2) How are the two streams of low-energy spots linked with each other and how will the periodicity of tip leakage flow unsteadiness take its place? Figures 10 and 11 in the next two paragraphs will illustrate these two mechanisms.

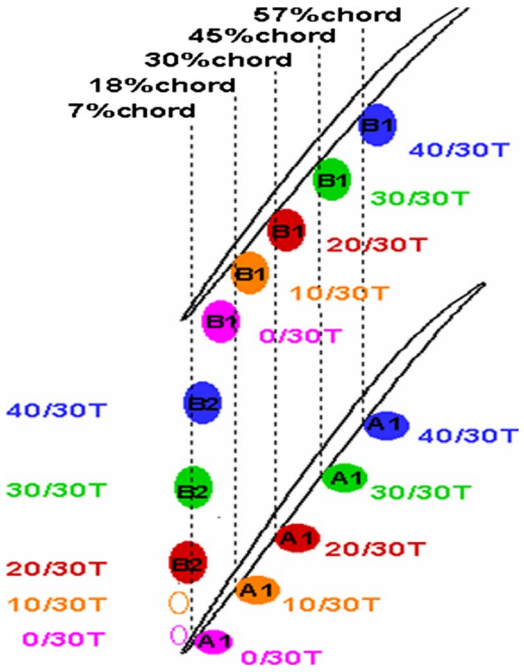

Fig. 9 Schematic of the unsteady process of self-induced tip leakage flow

Figure 10 is a contour plot of time-accurate velocity perturbation of tip leakage flow, which is the difference between the tip leakage flow velocity at each instant during the entire oscillating period and the averaged tip leakage flow velocity over the same period. The philosophy behind this plot is that the low-pressure spot (A1) at the pressure surface can only create pressure perturbation on top of the background pressure, and thus its influence can be clearly seen in velocity perturbation in tip leakage flow. The six dotted lines on the plot indicate the six time instants of Fig. 8. In order to demonstrate the influence of the pressure perturbation (A1), as well as the low-energy spot (B1) on the tip leakage flow, the locations of A1 at the time instants are read from Fig. 8(*c*) and added onto Fig. 10 using black circles. The local minima of velocity perturbation of the tip leakage flow are marked

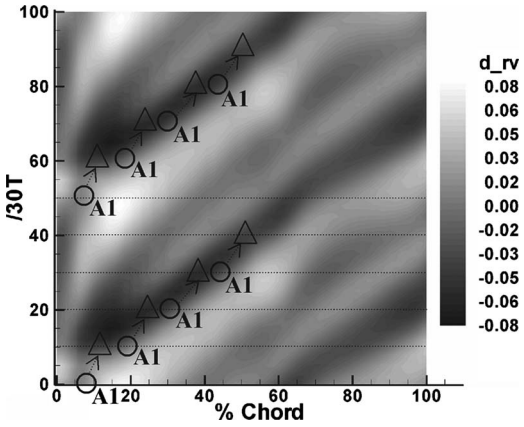

Fig. 10 Contour plot of velocity perturbation of tip leakage flow

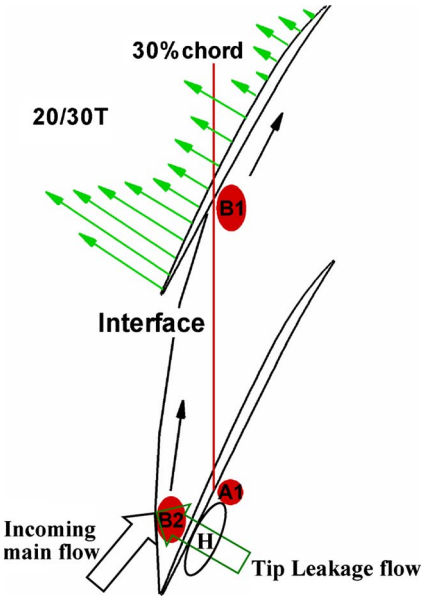

Fig. 11 Schematic of formation of B2 at 20/30 T with an addition of instantaneous velocity of tip leakage flow

as triangles. One can see that as the A1 (and B1) propagates downstream along the pressure surface, it reduces the velocity of tip leakage flow accordingly (but with a time lag as illustrated by the short dotted arrow lines), demonstrating the reaction of blade loading to the tip leakage flow.

The tip leakage flow impinges with the incoming main flow, and thus creates a stream of low-energy spots (B2) that travel across the blade passage. This process can be seen in Fig. 8(*b*) and further illustrated in Fig. 11. Figure 11 takes the snapshot of Fig. 8(*a*) at the time instant of 20/30 T, together with instantaneous velocity vectors of tip leakage flow (marked by the arrows along the blade chord). It can be seen that once the low-pressure spot moves away from the leading edge, the high blade loading due to the high pressure in the first 20% of the chord (copied from Fig. 8(*a*) and marked here as H in the ovals) creates strong tip leakage flow. As illustrated, the low-energy spot (B2) is a result of this strong tip leakage flow interacting with the incoming main flow. The similar interaction repeats at other time instants. Therefore, as shown in Fig. 8 and illustrated in Fig. 9, while the low-pressure spot A1 moves downstream, B2 moves across the blade passage and creates the second stream of the low-energy spots. Once the second stream of low-energy spots (B2) arrives at the pressure surface, the first stream A1 smears with the high-pressure background. The B2 turns itself to B1 seamlessly and a new period of oscillation thus starts. This process is qualitatively the same as what happened in the low-speed compressor in Ref. [12].

From the above description of the unsteady process, one can see that the onset of self-induced unsteadiness depends on whether the low-energy tip leakage flow is strong enough to alter the pressure distribution on the neighboring pressure surface significantly. However, this is closely related to the incoming main flow. If the incoming flow is reduced, the blade loading at the tip region increases, which in turn creates stronger tip leakage flow and thus the unsteadiness is more likely to happen. In other words, the incoming main flow generates the blade loading, which drives the tip leakage flow that then counteracts on the blade loading if its influence is stronger enough. In short, the dynamic interaction between the tip leakage flow and the incoming flow plays a decisive role in the onset of self-induced unsteadiness.

3.3 The Influence of Tip Clearance Sizes. In order to further verify the proposed mechanism that the initiation of the self-induced unsteady tip leakage flow is indeed attributed to the dynamic interaction between two driving forces, the incoming main flow and the tip leakage flow, we test it by varying one of the "forces" while keeping the other unchanged. This is done by comparing the results from different tip clearance sizes at the same incoming flow rate. The relative total pressure coefficient distribution with the same mass flow rate ($0.99m_{\text{choke}}$) for tip clearances of 0.25%, 1.1%, and 2.2% tip blade chords, corresponding with S_1, S_2, and U_3 (unsteady) points in Fig. 5, is shown in Fig. 12. Since larger tip clearance size produces stronger tip leakage flow, with 2.2% tip chord the region of influence by the tip leakage flow not only reaches the pressure side of the neighboring blade, but also penetrates further down along the span of the blade. It is therefore not surprised that only the case with 2.2% tip chord exhibits the unsteadiness at this mass flow rate, while the other two cases are steady.

3.4 Correlation of Onset Conditions. As indicated in Fig. 5, there is a threshold value of mass flow rate for the onset of tip leakage flow unsteadiness for tip clearances of 1.1% and 2.2% of tip chord. Figure 13 provides relative total pressure coefficient distributions at the blade tip right before and after the threshold values for tip clearances of 2.2% tip chord. It can be seen that from steady to unsteady, both the location of the interface between the incoming flow and TLF and the region of influence by TLF vary gradually. This actually is good news from flow control point of view, because it means no hysteresis associated with this change in flow dynamics.

We now propose a means to correlate the onset conditions for the self-induced unsteady tip leakage flow. Since the interface between incoming main flow and tip leakage flow is a consequence of the impact of these two flows in the tip clearance re-

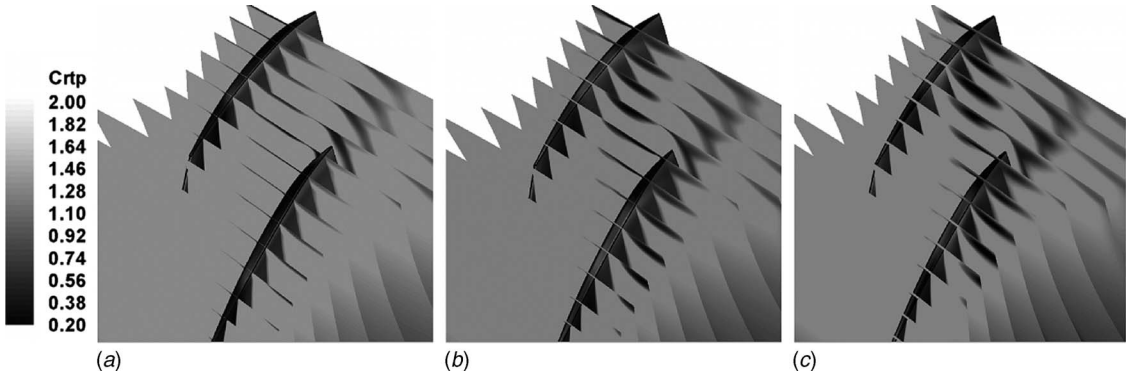

Fig. 12 Relative total pressure coefficient distribution for operating conditions S_1, S_2, and U_3. (*a*) 3D, steady (S_1); (*b*) 3D, steady (S_2); and (*c*) 3D, unsteady (U_3).

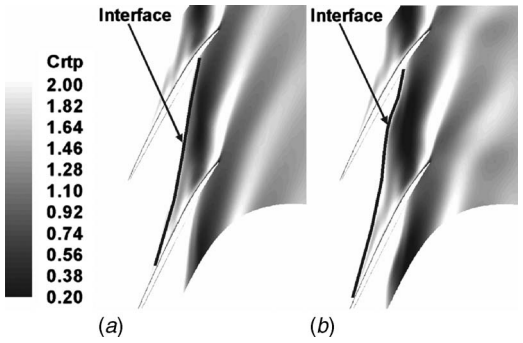

Fig. 13 Relative total pressure coefficient distribution at 98.4% span for tip clearance of 2.2% tip chord. (*a*) Steady (S_3) and (*b*) unsteady (U_3).

gion, we will use the ratio of two momenta as one of the parameters for our correlation. The ratio of M_{Tp} to M_{Is} is

$$R = \frac{M_{Tp}}{M_{Is}} = \frac{M_{Tt}\cos\alpha - M_{Ta}\sin\alpha}{M_{Ia}\cos\alpha + M_{It}\sin\alpha}$$

where subscripts I, T, s, p, t, a, and r are used to represent incoming flow, tip leakage flow, streamwise direction, perpendicular to streamwise direction, tangential direction, axial direction, and radial direction. The other parameter is the dimensionless tip clearance, which is the ratio of tip clearance to the blade height. The available CFD data of two different rotors, NASA Rotor 67 and NASA Rotor 37, are considered. The data for Rotor 37 are taken from Ref. [15]. Figure 14 shows the correlation between the dimensionless tip clearance size and the momentum ratio for onset conditions of unsteady tip leakage flow. The limit curve in this figure can qualitatively predict the occurrence of unsteady TLF. The operating points located at the upper side of the curve are unsteady cases, and those in the lower side of the curve are steady. This figure also indicates that as the tip clearance size increases, the critical momentum ratio decreases. In other words, self-induced unsteadiness with a larger tip clearance size appears earlier as the mass flow rate is throttled.

4 Discussions

4.1 The Role of Shock Wave. Carefully examining Fig. 8(*a*), one can notice that the location of the shock on the suction surface hardly oscillates during the entire period of unsteadiness. Figure 15 depicts the distribution of pressure coefficient on the suction surface for all six time instants used in Fig. 8(*a*). Both the location and the strength of this shock only slightly vary with time. This brings an interesting question on the role of shock wave in the

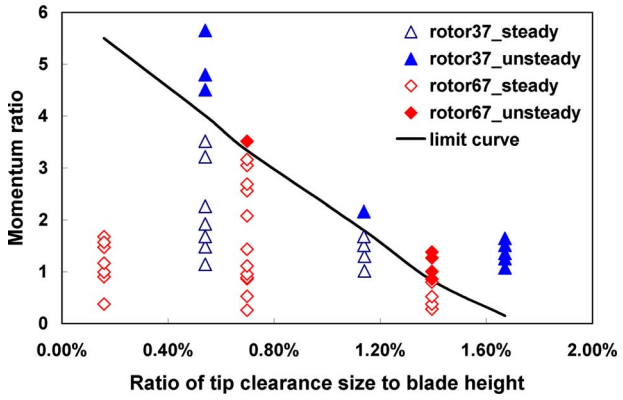

Fig. 14 Correlation for unsteadiness of tip leakage flow

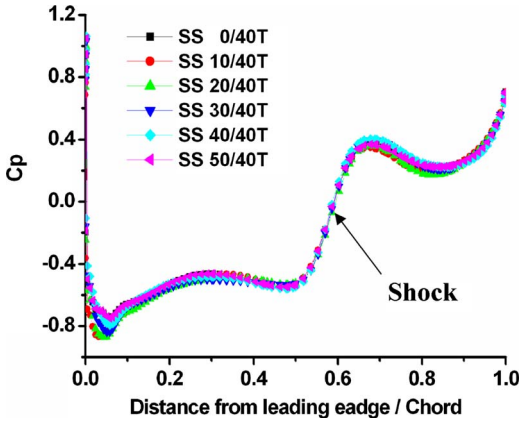

Fig. 15 Pressure coefficient distribution on blade suction surface at six time instants

self-induced unsteadiness of tip leakage flow.

To further investigate the role of shock wave, the rms distribution across the blade passage is examined. In Fig. 16, the highest unsteadiness is located at A and B, which are the initial position of the tip leakage vortex and the trajectory of the tip leakage vortex, respectively. C is the region for fluctuation of the detached shock wave in front of the leading edge. D is the unsteady region where the tip leakage vortex interacts with the detached shock wave. Obviously, the shock wave oscillates less than the tip leakage vortex.

There are two mechanisms proposed in literatures that concern the role of shock wave in unsteadiness. Yamada et al. [10] found that it is the breakdown of the tip clearance vortex occurring in the Rotor 37 that resulted in self-sustained flow oscillation in the tip leakage flow field. Bergner et al. [6] and Hah et al. [7] argued that the occurrence of unsteady fluctuation is due to the interaction of tip leakage vortex with the shock wave. Both mechanisms are checked carefully against what we found in Rotor 67.

First of all, we realized that Yamada et al. [10] utilized Reynolds-averaged Navier-Stokes (RANS) solver for their study, so do we in the present paper. Hence, when comparing our results with theirs, if there is any qualitative difference in simulation results, it is most likely related to physics of flow, not the computation scheme. Figure 17 depicts the 3D normalized absolute vorticity magnitude (ξ_n) distribution from our simulation and shows

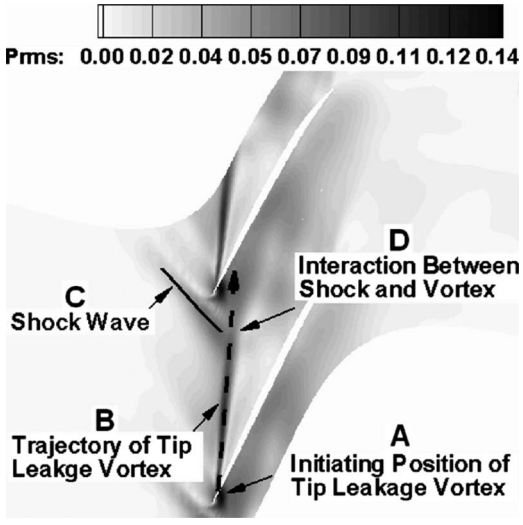

Fig. 16 Static pressure rms distribution for 99% span at T_2 operating condition for 1.1% tip blade chord

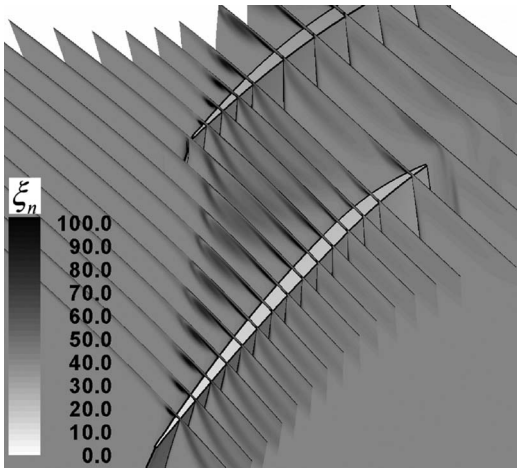

Fig. 17 3D normalized absolute vorticity magnitude distribution at T_2 operating condition

that the vortex does not break down because the magnitude of absolute vorticity does not drop drastically when its trajectory crosses the shock wave. This is fundamentally different from the results in Ref. [10]. Carefully examining Fig. 12 of Ref. [10], we notice that the vortex breakdown caused by the shock behaved randomly; that is, it did not possess any periodic pattern. Yet, it was reported in Ref. [10] that the frequency of unsteadiness was about 60% BPF, amazingly close to what we find in the present paper for Rotor 67. These apparently contradicting phenomena make us believe that the vortex breakdown in Rotor 37 might be responsible for turbulence unsteadiness, which should be random and broadband. The unsteadiness associated with 60% BPF might be due to another mechanism, which could be the same self-induced unsteadiness as what we find in Rotor 67. Both the turbulence unsteadiness and the self-induced unsteadiness might be present in the results of Rotor 37.

In the present study, the region where the vortex and the shock interact (region D in Fig. 16) depicts less rms level than the tip leakage vortex itself. Hah et al. [7] reported that while their RANS solver obtained qualitatively similar result as Fig. 16 for their rotor (see their Fig. 6 in Ref. [6]), the large-eddy-simulation (LES) solver produced rms distribution that matched with experimental results [6] better. But, Hah et al. [7] also reported that "the pressure oscillation from the single passage analysis shown in Fig. 8 is rather random at this operating condition and any distinct frequency could not be clearly identified." This contradicted with the experimental results in Ref. [6], which showed that the vortex trajectory alternated blade by blade, inferring that there was a characteristic frequency at roughly 50% BPF. All these seem pointing to the same direction: Both turbulence unsteadiness and self-induced unsteadiness might coexist in the rotor studied in Refs. [6,7] as well. There is a good chance that such coexistence may also be true for Rotor 67. However, without experiments and LES simulation, we cannot verify it in this paper. Realizing that vortex breakdown is an extreme case of shock/vortex interaction, we tend to believe that shock/vortex interaction produces turbulence unsteadiness and that the coexistence of turbulence unsteadiness and self-induced unsteadiness may be very common in compressors with shocks. Further research is needed.

4.2 Link to Stall Inception. According to Refs. [2,16], the spike disturbance is a result of dynamic interaction of three driving forces: the incoming main flow, the tip leakage flow, and the reversed backflow. The self-induced unsteady tip leakage flow partially shares the same dynamics with the spike disturbance, because as we proposed in Sec. 3, such unsteadiness results from the interaction of incoming flow and the tip leakage flow, two out of the three driving forces for the spike disturbance. This also explains why numerical and experimental data of previous researches [3,15] demonstrated that the suppression of the unsteadiness of tip leakage flow could extend the stability margin of both low-speed and high-speed compressors.

The proposed mechanism offers a new view angle for compressor design such as sweep and dihedral and stability enhancement such as casing treatment. By carefully designing the geometry, the designers should be able to make the dynamic interaction behave in a favorite manner at will, so that the compressor becomes more robust. This is the planned future work for the authors of the present paper.

5 Conclusions

In this paper, unsteady numerical simulation of Rotor 67, a transonic fan rotor, is performed. The goal is to investigate the originating mechanism of the self-induced unsteadiness in tip leakage flows in a transonic environment. The findings can be summarized as follows.

1. The self-induced unsteadiness of the tip leakage flow in this high-speed fan rotor is a result of dynamic interaction of two driving forces: the incoming main flow and the tip leakage flow. These two flows impinge with each other at the tip region and form an interface that separates the two flows. On one hand, behind the interface, if the tip leakage flow is stronger enough to cast a low-energy spot on the pressure side of the neighboring blade, the unsteadiness would be initiated as the low-energy spots move downstream, which in turn cause the time variation of blade loading. On the other hand, the changing blade loading makes the tip leakage flow velocity oscillating, which interacts with the incoming main flow to create the second low-energy spots across the blade passage. When the second stream of low-energy spots arrives at the pressure surface, the first stream smears with the high-pressure background and a new period of oscillation thus starts.
2. The proposed originating mechanism of the self-induced unsteady tip leakage flow is tested by varying the tip clearance sizes while keeping the incoming main flow the same.
3. A correlation based on momentum ratio between the main flow and the tip leakage flow is proposed. It indicates that the momentum ratio can be one of the factors that dominate the self-induced unsteadiness of the tip region.

Acknowledgment

This work was supported by the National Basic Research Program of China Grant No. 2007CB210104 and the National Science Foundation of China Grant No. 50736007. These supports are gratefully acknowledged. F.L. also appreciates the support of Tri-State University through Lilly Faculty Development Grant.

Nomenclature

P = static pressure (Pa)

$\bar{P}$ = time-averaged static pressure (Pa)

P_{rt} = relative total pressure (Pa)

P_{ref} = reference pressure (Pa)

C_p = static pressure coefficient, $C_p=(P-P_{ref})/(0.5\rho U_m^2)$

C_{rtp} = relative total pressure coefficient, $C_{rtp}=(P_{rt}-P_{ref})/(0.5\rho U_m^2)$

P_{rms} = static pressure root-mean-square, $P_{rms}=\sqrt{1/N\sum_{i=0}^{N-1}(P(t)-\bar{P})^2}/0.5\rho U_m^2$

ΔC_p = static pressure coefficient difference

U_m = blade speed at the mean rotor diameter (m/s)

T = rotor blade passing period (s)

M = momentum (N/s)

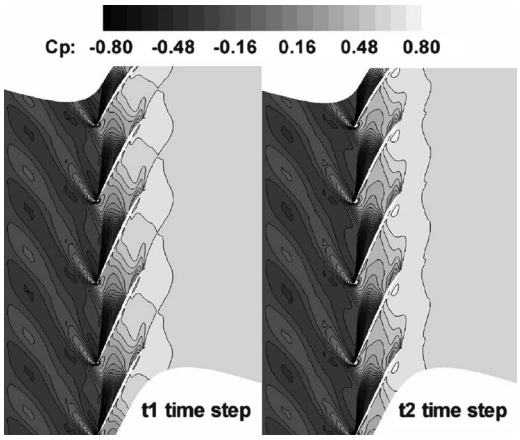

Fig. 18 Instant static pressure coefficient contours taken from 99% span at T2 operating condition in multiblade passages

m_{choke} = mass flow rate at choke point (kg/s)

Greek Symbols

α = angle between streamwise and axial directions
ξ = absolute vorticity magnitude (rad/s)
ω = rotor angular velocity (rad/s)
ξ_n = normalized absolute vorticity magnitude, $\xi_n = |\xi|/2\omega$
ρ = r density (kg/m^3)
τ = ratio of tip clearance size to tip blade chord

Abbreviations

TLF = tip leakage flow

Appendix

One case of self-induced unsteady tip leakage flow in multiblade passages is investigated to demonstrate that it is sufficient to use single blade passage model in this research. One quarter of the annulus of Rotor 67 is chosen. The operating condition and the tip clearance are the same as those in Fig. 8. The unsteady flow fields for the entire oscillating period are captured, and two of them at two different time instants are depicted in Fig. 18. By comparison among the blade passages, one can see that the flow field in each blade passage is identical at every time instants. This indicates that the self-induced unsteadiness does not involve cross-passage dynamics. Single blade passage model is sufficient when investigating the characteristics of self-induced unsteady tip leakage flow.

References

[1] Wisler, D. C., 1985, "Loss Reduction in Axial-Flow Compressor Through Low-Speed Model Testing," ASME J. Turbomach., **107**, pp. 354–363.
[2] Lin, F., Zhang, J. X., Chen, J. Y., and Nie, C. Q., 2008, "Flow Structure of Short Length Scale Disturbance in an Axial Flow Compressor," J. Propul. Power, **24**(6), pp. 1301–1308.
[3] Tong, Z. T., Lin, F., Chen, J. Y., and Nie, C. Q., 2007, "The Self-Induced Unsteadiness of Tip Leakage Vortex and Its Effect on Compressor Stall Inception," ASME Paper No. GT2007-27010.
[4] Mailach, R., 1999, "Experimental Investigation of Rotating Instability in a Low-Speed Research Compressor," Third European Conference on Turbomachinery-Fluid Dynamics and Thermodynamics, London, GB, Mar. 2–5.
[5] Marz, J., Hah, C., and Neise, W., 2001, "An Experimental and Numerical Investigation Into the Mechanisms of Rotating Instability," ASME Paper No. 2001-GT-0536.
[6] Bergner, J., Kinzel, M., Schiffer, H., and Hah, C., 2006, "Short Length-Scale Rotating Inception in a Transonic Axial Compressor-Experimental Investigation," ASME Paper No. GT2006-90209.
[7] Hah, C., Bergner, J., and Schiffer, H., 2006, "Short Length-Scale Rotating Stall Inception in a Transonic Axial Compressor—Criteria and Mechanisms," ASME Paper No. GT2006-90045.
[8] Furukawa, M., Inoue, M., Saiki, K., and Yamada, K., 1999, "The Role of Tip Leakage Vortex Breakdown in Compressor Rotor Aerodynamics," ASME J. Turbomach., **121**, pp. 469–480.
[9] Furukawa, M., Saiki, K., Yamada, K., and Inoue, M., 2000, "Unsteady Flow Behavior Due to Breakdown of Tip Leakage Vortex in an Axial Compressor Rotor at Near-Stall Condition," ASME Paper No. 2000-GT-666.
[10] Yamada, K., Furukawa, M., Inoue, M., and Funazaki, K., 2004, "Unsteady Three-Dimensional Flow Phenomena Due to Breakdown of Tip Leakage Vortex in a Transonic Axial Compressor Rotor," ASME Paper No. GT2004-53745.
[11] Zhang, H. W., Deng, X. Y., Lin, F., Chen, J. Y., and Huang, W. G., 2005, "Unsteady Tip Leakage Flow in an Isolated Axial Compressor Rotor," J. Therm. Sci., **14**(3), pp. 211–219.
[12] Zhang, H. W., Deng, X. Y., Lin, F., Chen J. Y., and Huang, W. G., 2006, "A Study on the Mechanism of Tip Leakage Flow Unsteadiness in an Isolated Compressor Rotor," ASME Paper No. GT2006-91123.
[13] Adamczyk, J. J., Celestina, M. L., and Greitzer, E. M., 1993, "The Role of Tip Clearance in High-Speed Fan Stall," ASME J. Turbomach., **115**, pp. 28–39.
[14] Strazisar, A. J., Wood, J. R., Hathaway, M. D., and Suder, K. L., 1989, "Laser Anemometer Measurements in a Transonic Axial-Flow Fan Rotor," NASA, Report No. TP 2879.
[15] Geng, S. J., 2007, "Numerical Study on the Unsteady Response of Compressor Tip Leakage Flow to Discrete Micro Tip Injection and Its Effect on Stability Enhancement," Ph.D. thesis, Graduate School of the Chinese Academy of Sciences, Beijing, China.
[16] Vo, H. D., Tan, C. S., and Greitzer, E. M., 2005, "Criteria for Spike Initiated Rotating Stall," ASME Paper No. GT2005-68374.